The role of the leading edge vortex in lift augmentation of steadily revolving wings: A change in perspective

Article · July 2017

DOI: 10.1098/rsif.2017.0159

CITATIONS
48

READS
726

2 authors:

Mostafa R. A. Nabawy
The University of Manchester
67 PUBLICATIONS **576** CITATIONS

SEE PROFILE

William James Crowther
The University of Manchester
90 PUBLICATIONS **1,113** CITATIONS

SEE PROFILE

INTERFACE

rsif.royalsocietypublishing.org

Perspective

Cite this article: Nabawy MRA, Crowther WJ. 2017 The role of the leading edge vortex in lift augmentation of steadily revolving wings: a change in perspective. *J. R. Soc. Interface* **14**: 20170159.
http://dx.doi.org/10.1098/rsif.2017.0159

Received: 3 March 2017
Accepted: 28 June 2017

Subject Category:
Life Sciences–Engineering interface

Subject Areas:
biomechanics, biomimetics

Keywords:
insect flight, leading edge vortex, aerodynamics, revolving wings, flapping flight, absence of stall

Author for correspondence:
Mostafa R. A. Nabawy
e-mail: mostafa.ahmednabawy@manchester.ac.uk

THE ROYAL SOCIETY PUBLISHING

The role of the leading edge vortex in lift augmentation of steadily revolving wings: a change in perspective

Mostafa R. A. Nabawy and William J. Crowther

School of Mechanical, Aerospace and Civil Engineering, University of Manchester, Manchester M13 9PL, UK

MRAN, 0000-0002-4252-1635

The presence of a stable leading edge vortex (LEV) on steadily revolving wings increases the maximum lift coefficient that can be generated from the wing and its role is important to understanding natural flyers and flapping wing vehicles. In this paper, the role of LEV in lift augmentation is discussed under two hypotheses referred to as 'additional lift' and 'absence of stall'. The 'additional lift' hypothesis represents the traditional view. It presumes that an additional suction/circulation from the LEV increases the lift above that of a potential flow solution. This behaviour may be represented through either the 'Polhamus leading edge suction' model or the so-called 'trapped vortex' model. The 'absence of stall' hypothesis is a more recent contender that presumes that the LEV prevents stall at high angles of attack where flow separation would normally occur. This behaviour is represented through the so-called 'normal force' model. We show that all three models can be written in the form of the same potential flow kernel with modifiers to account for the presence of a LEV. The modelling is built on previous work on quasi-steady models for hovering wings such that model parameters are determined from first principles, which allows a fair comparison between the models themselves, and the models and experimental data. We show that the two models which directly include the LEV as a lift generating component are built on a physical picture that does not represent the available experimental data. The simpler 'normal force' model, which does not explicitly model the LEV, performs best against data in the literature. We conclude that under steady conditions the LEV as an 'absence of stall' model/mechanism is the most satisfying explanation for observed aerodynamic behaviour.

1. Introduction

1.1. Background

The aim of this paper is to provide a contribution to the debate on the role of the leading edge vortex (LEV) in lift production in revolving wings based on rigorous comparison of low-order modelling predictions with relevant experimental and numerical data. While high-order computational fluid dynamics (CFD) methods are now able to accurately tackle flapping wing flows, the value of low-order analytical models remains in that they provide insight into the flow physics that are not available from higher-order methods. The existence of a LEV on insect-like wings at low Reynolds numbers and the improvement in overall lift production associated with its presence is considered scientific fact [1–5]. However, there remain significant differences in opinion as to the *actual mechanism by which the lift is enhanced*. We group the different views on the role of the LEV in lift production under two hypotheses, namely the 'additional lift' hypothesis and the 'absence of stall' hypothesis. In the additional lift view, the additional circulation/suction from the LEV increases the lift above that of the nominal potential flow solution. In the absence of stall view, the LEV allows the flow to approximate the potential flow solution at high angles of

attack at which the flow would normally be fully separated in a flow without a LEV.

Given the two hypotheses above, why does it matter which is more representative of the physics if the final outcome is the same? The reason is that the role of the LEV fundamentally affects the way we understand how insect-like wings at low Reynolds number work and hence our experimental approach to understanding insect flight and the design of engineered flapping wing vehicles. The choice also clearly affects our selection of models to represent the flow. If the 'additional lift' hypothesis is true then we should expect our models to explicitly include terms for lift due to a circulation contribution from the LEV. There is, of course, a third alternative in that neither hypothesis is true, or that the actual situation is a combination of both, depending on the exact conditions. Nonetheless, the activity of trying to assess the validity of the different hypotheses remains instructive in that it provides structure to the debate which we believe is helpful.

While the context for the work is flapping wing aerodynamics, it is important to stress we explicitly focus here on quasi-steady revolving wing aerodynamics. This in itself may be considered contentious if the LEV is assumed to be an unsteady phenomenon and hence cannot be fully captured by steady aerodynamic models. Indeed, if we allow unsteady effects, then in addition to the LEV as 'additional lift' and 'absence of stall' hypotheses, we could include a further hypothesis as LEV as 'all the lift' in which a wing with no bound circulation instantaneously traps a vortex and generates a finite amount of lift. We take the view that the quasi-steady assumption is both valid and useful. The quasi-steady assumption greatly reduces the size of the parameter space and there is a significant body of CFD and experimental work to which theory can be compared. It is understood that there will be unsteady effects due to stroke reversal in reciprocating rather than revolving motion. However, for the most important case of normal hovering with symmetric half-strokes, these effects are relatively small compared with the quasi-steady effects. Hence, with some caution, the arguments developed here for revolving motion retain core relevance when transferred to reciprocating motion.

Finally, as a comment on the research method adopted in this paper, we recognize that use of low-order models calibrated against experimental or CFD data clearly cannot be used to infer structure in the data from which they are calibrated. In the present work we thus adopt a first principles modelling approach based on the authors' previous work in which model parameters are built up from geometry, kinematics and physics. These models are then properly predictive in the sense that they may reasonably be used for predicting results for which experimental data does not exist. We now provide a more detailed technical description of the LEV and the current state of knowledge.

1.2. The leading edge vortex

A LEV is known to form on thin wings with moderate aspect ratio (approx. 3), steadily revolving at high angles of attack and low Reynolds number of $O(10^4)$ or lower, figure 1. The LEV is stable in that its location remains near the leading edge and it does not grow with time; this allows the flow over the upper surface of the wing to separate at the leading edge but then reattach before the trailing edge, figure 1*a*. A wing with a stable LEV is thus able to satisfy the Kutta condition at the trailing edge at angles of attack beyond which classical stall would occur for wings where no LEV is present, and consequently a substantial enhancement of the wing lift coefficient is achieved [1].

There has been substantial research within the last two decades directed at understanding the aerodynamic characteristics of revolving and flapping wings at Reynolds numbers relevant to insect/vertebrate flight. Some of these studies concentrated on flow visualization to identify the flow topology, analyse circulation characteristics and determine possible causes for the stability of the LEV [2–14], while others concentrated on measuring the generated forces for different wing morphologies and kinematics [15–22]. Note that for completeness we refer to both steady and unsteady studies here. The identified LEV topologies were shown to vary from a conical form with a substantial spanwise flow at the vortex core (as that observed on model hawkmoth wings at Reynolds number from 10^3 to 10^4 [2], figure 1*b*) to a cylindrical form with a substantially weaker corewise vortex flow (as that observed on fruit fly and thrip wings at Reynolds number of the order 10^2 and 10^1 [3,4]). However, these differences in the LEV flow topologies were not reflected in differences in the measured lift polars [1,16,23], suggesting that the LEV is playing an aerodynamic role that it is to some extent independent of its shape under quasi-steady conditions.

Pitt Ford & Babinsky [24] used the 'trapped vortex' model to investigate the relation between lift production and LEV formation in unsteady wing motions. They proposed that most of the lift is due to the circulation contained in the LEV rather than the bound vortex. This conclusion was based on a best fit approach conducted between the 'trapped vortex' model and their experimental measurements. However, their experimental measurements were for an unsteady *translating* wing case at 15° angle of attack and hence the experimental conditions do not generally represent the revolving/flapping wing scenario. Nevertheless, together with a consortium of different groups, this work was followed by experimental measurements for unsteady motions of translating and revolving rectangular wings (both surging and pitching) at 45° angle of attack [25–27]. It was found that unlike the translational case, the revolving wing motion allowed an *attached* LEV to form on top of the wing. They also found that this attached vortex did not result in significantly higher lift coefficient compared to the detached vortex from the translating unsteady case [26]. This is different from the quasi-steady cases where it is well established that the attached LEV in revolving motion allows significantly higher lift coefficient values compared to the detached LEV in translational motion (e.g. Usherwood & Ellington [15] and Sane [1]). Later, Phillips *et al*. [28] adopted the findings of Pitt Ford and Babinsky for unsteady translating wings, and calculated the lift based on the circulation contained only within the formed LEV for a series of flapping wings with different Rossby number (note that translating motion corresponds to infinite Rossby number while revolving motion corresponds to a finite Rossby number value equivalent to the ratio of the radius of gyration to the mean chord [19]). The LEV lift coefficient was found to *increase* as the Rossby number increases [28], a result which is inconsistent with previous experimental force measurements [19] and numerical simulation [29]. Thus, while unsteady effects

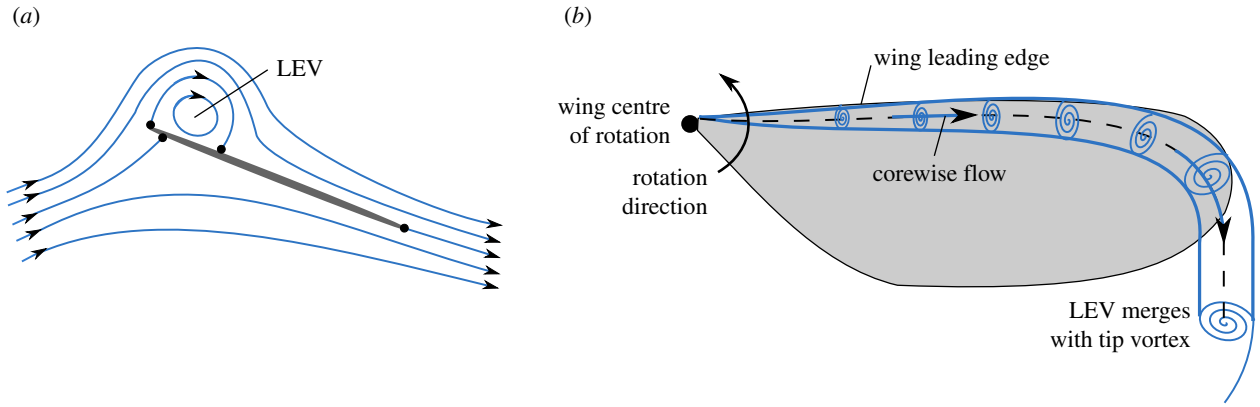

Figure 1. (*a*) Schematic showing the simplest valid LEV structure for a cylindrical vortex—cross-section view. The LEV is stable at high angles of attack with flow reattachment on the upper surface and satisfaction of the Kutta condition at the trailing edge. The black dots represent stagnation points. (*b*) An idealized top view schematic illustrating a conical LEV topology for a steadily revolving wing with a focus at the root. This topology has been observed at Reynolds numbers of $O(10^3-10^4)$ [2,3]. (Online version in colour.)

undoubtedly play an effect in establishing the flow field, the evidence for this in the literature is incomplete.

The presence of a LEV was first identified by Maxworthy while conducting experiments on the Weis-Fogh 'clap and fling' mechanism [30]. Subsequently, the role of the LEV in insect aerodynamics was developed by Ellington and his group [2], who proposed the LEV as a 'dynamic/delayed stall' mechanism. This description has persisted despite the fact that dynamic stall is an unsteady mechanism that cannot be maintained for an indefinite period and that the vortex created during a dynamic stall convects directly after the wing starts to translate [3,31,32]. Furthermore, many revolving wing experiments [15–23] demonstrated that the LEV is a *steady* aerodynamic mechanism that can be maintained indefinitely on revolving wings. Recently, Kruyt *et al*. [33] experimentally demonstrated that stall is prevented on revolving wings as long as they have an aspect ratio (defined from centre of revolution) that does not exceed four, a number that most insect and hummingbird wings are clustered around.

2. Models

2.1. Overview

In this section, we introduce three low-order models that have previously been used to model steady wing flows, namely the 'normal force' model, the 'leading edge suction' model and the 'trapped vortex' model. A contribution of this section is to show that all three of these models can be expressed in the form of a common potential flow model corrected for three-dimensional (3D) effects, plus additional model specific corrections to account for operation at high angle of attack or the addition of vortex lift. The fact that these apparently dissimilar models can all be expressed with a common core allows attention to be focused on the physical contribution of the LEV in the model. We first present the potential flow model which provides the core of the three models under consideration.

2.2. Potential flow model

The classical potential flow model is based on assumption of fully attached flow to the wing up to 90° angle of attack. In an idealized two-dimensional (2D) flow, the lift coefficient, C_l, for a flat plate is expressed as

$$C_l = 2\pi \sin\alpha = C_{L\alpha,2D} \sin\alpha, \tag{2.1}$$

where $C_{L\alpha,2D}$ is the 2D aerofoil lift curve slope and α is the angle of attack. For a 3D wing, the lift coefficient, C_L, is therefore expressed as

$$C_L = C_{L\alpha,3D} \sin\alpha = (C_{L\alpha,3D} \sin\alpha \cos\alpha) \sec\alpha, \tag{2.2}$$

where $C_{L\alpha,3D}$ is the 2D lift curve slope corrected for appropriate geometry and kinematic effects (see §2.6). Note that the right-hand side of equation (2.2) is written in this form to provide basis of comparison with the 'normal force' model that will be discussed later. The potential flow model is useful at low angles of attack, but clearly non-physical at high angles of attack approaching 90°, where geometry dictates that the lift must tend towards zero when the wing is perpendicular to the flow.

2.3. Normal force model

The 2D form of normal force model is expressed as the potential flow model multiplied by a cos α term [34,35]:

$$C_l = \pi \sin 2\alpha = \tfrac{C_{L\alpha,2D}}{2} \sin 2\alpha = C_{L\alpha,2D} \sin\alpha \cos\alpha. \tag{2.3}$$

Consequently from equation (2.3), the 3D wing form is expressed as

$$C_L = C_{L\alpha,3D} \sin\alpha \cos\alpha. \tag{2.4}$$

The cos α term may be thought of as a geometric correction to the potential flow model that drives the lift to zero at 90° angle of attack as required by physics. The model structure of equation (2.4) written in terms of a normal force coefficient, C_N, is

$$\left.\begin{aligned} C_N &= \hat{C}_N \sin\alpha, \\ C_L &= C_N \cos\alpha \\ \text{and} \quad C_D &= C_N \sin\alpha, \end{aligned}\right\} \tag{2.5}$$

where $\hat{C}_N$ is the normal force coefficient amplitude and C_D is the 3D wing drag coefficient. Thus the model implicitly assumes that the overall aerodynamic force is *normal* to the wing chord [15,18,36–41]. As an aside, this requires that: (1) the wing is an infinitesimally thin flat plate, and hence there is no chordwise component to the integrated surface

pressure force and (2) the chordwise tangential force due to skin friction is negligible compared with the integrated surface pressure force acting normal to the chord [18]. Note that the normal force model has historically been used to represent the un-stalled 2D aerofoil lift coefficient of wings operating at high angles of attack within the helicopter and fixed wing aerodynamics literature [34,35]. Later, various models based on the normal force assumption have been widely used to represent the quasi-steady aerodynamics of revolving/flapping wings [15,18,36–41].

2.4. Leading edge suction model

The leading edge suction model is based on the so-called 'leading edge suction analogy' proposed by Polhamus for delta wings [42]. The conical LEV created on laminar revolving/flapping wings is similar in form to the LEV observed over delta wings at subsonic speeds and high angles of attack. This prompted several researchers [1,15,41,43] to use the 'leading edge suction' model for delta wings to analyse the revolving/flapping wing problem. Note that while at first sight revolving/flapping wings and steady delta wings appear quite different, the key similarity is that in each a stable LEV is able to form. For the delta wing it is the leading edge sweep which provides the stabilizing spanwise pressure gradient; for the flapping/revolving wing it is the spanwise velocity distribution that provides the stabilizing pressure gradient [19]. The 'leading edge suction' model is formulated on the basis that the leading edge flow separation that creates the LEV causes a loss of the leading edge suction that would have otherwise been generated had the flow remained attached at the leading edge. The lift is thus comprised of two components. The first is the potential flow lift but with zero leading edge suction. The second is a vortex lift related to the 'missing' leading edge suction associated with the potential flow. Polhamus did not attempt to provide a theoretical proof of his analogy; however, it has historically proved useful in estimating aerodynamic force coefficients on delta wings within their normal operating range of angles of attack ($\alpha \leq 25^\circ$). It is worth noting that this angle of attack limit is below the typical maximum angle of attack of around 45° up to which insect wings operate. The model can be expressed for 3D wings as follows [42]:

$$C_\mathrm{L} = \underbrace{C_{\mathrm{L}\alpha,\mathrm{3D}} \sin\alpha \cos^2\alpha}_{\text{potential lift},C_{\mathrm{L},p}} + \underbrace{\left(C_{\mathrm{L}\alpha,\mathrm{3D}} - \frac{kC_{\mathrm{L}\alpha,\mathrm{3D}}^2}{\pi \mathrm{AR}}\right)\frac{1}{\cos\Lambda}\sin^2\alpha\cos\alpha}_{\text{vortex lift},C_{\mathrm{L},v}}, \tag{2.6}$$

where Λ is the wing sweep angle (which is assumed zero for revolving wings), AR is the wing aspect ratio and k is the so-called 'k-factor' included to correct for the difference in efficiency between assumed ideal uniform downwash distribution and real downwash distribution [44,45]. In order to make direct comparisons with other models of interest, we rearrange equation (2.6) as follows:

$$C_\mathrm{L} = (C_{\mathrm{L}\alpha,\mathrm{3D}} \sin\alpha\cos\alpha)\underbrace{\left(\cos\alpha + \left(1 - \frac{k_\mathrm{ind}k_\mathrm{per}C_{\mathrm{L}\alpha,\mathrm{3D}}}{\pi \mathrm{AR}}\right)\sin\alpha\right)}_{K_\mathrm{Pol}(\alpha)}. \tag{2.7}$$

Note that to address the specific flow physics associated with revolving wings the k-factor is split into two components: k_ind to account for the non-uniform downwash effect and k_per to account for wake periodicity. The method for prediction of these parameters is based on the authors' previous work which may be found in [44].

2.5. Trapped vortex model

Following the work of Saffman & Sheffield [46], the so-called 'trapped vortex model' is based on steady, inviscid, incompressible and irrotational 2D potential flow over a flat plate with an embedded free vortex. Thus the model has similarity to the leading edge suction model; however in this present case the strength of the LEV is a *free* variable. This model is based on the well-known Joukowski transformation approach where the flow is mapped from a circle of radius a to a flat plate with a chord length of $4a$ inclined at an angle of attack α to the free stream, U [46,24]. Briefly, a free vortex element is included with a circulation Γ_free located at $\zeta = \rho e^{i\varphi}$ in the circle plane, where the radius ρ and the angle φ are user specified variables to define the free vortex location in the circle plane. An image vortex of equal but opposite sign to Γ_free is located at the inverse square point and a second vortex of equal circulation to Γ_free is located at the circle centre; thus, the circulations of image vortices cancel [24]. The Kutta condition is satisfied by equating the velocity to zero at $\zeta = a$. The magnitude of the bound circulation can be represented as [24]

$$\Gamma = 4\pi a U \sin\alpha + \Gamma_\mathrm{free}\frac{2a(a - \rho\cos\varphi)}{\rho^2 - 2a\rho\cos\varphi + a^2}. \tag{2.8}$$

The first term of the right-hand side of equation (2.8) is the well-known result for the bound circulation of a flat plate at incidence, whereas the second term accounts for the circulation added by the *trapped* free vortex (LEV) located at $\zeta = \rho e^{i\varphi}$. Expressing equation (2.8) in terms of the 2D lift coefficient gives

$$C_\mathrm{l} = \frac{\Gamma}{2aU} = 2\pi\sin\alpha + \underbrace{\frac{\Gamma_\mathrm{free}}{2aU}\frac{2(1 - (\rho/a)\cos\varphi)}{(\rho/a)^2 - 2(\rho/a)\cos\varphi + 1}}_{C_{\mathrm{Lfree,2D}}}. \tag{2.9}$$

The addition of a free vortex in the above results represents an additional *constant* increment in circulation at all angles of attack. Now, for a given chord, U and α, equation (2.9) becomes one equation in three unknowns (C_l, Γ_free and ζ); thus it cannot be used without further input to evaluate the lift, and either additional information or experimental data (as in [24]) needs to be used to define some of the unknown parameters. By analogy, equation (2.9) can be written to express the overall lift coefficient of the 3D wing as

$$C_\mathrm{L} = C_{\mathrm{L}\alpha,\mathrm{3D}}\sin\alpha + C_{\mathrm{Lfree,3D}}. \tag{2.10}$$

Note that the first term in equation (2.10) is the potential flow model as stated in equation (2.2). This is to be expected because the potential flow model is ultimately derived by the same Joukowski transformation approach. The free vortex contribution to lift as defined by the second term in equation (2.10) will ultimately depend on the strength of the LEV as a function of angle of attack. From fundamental considerations we know that the LEV strength will be zero at zero angle of attack and will increase with increasing angle of attack. From observation we also know that there is a limit to the size to which the LEV can grow as the angle of attack increases. Thus while we cannot calculate values for

the free vortex lift in equation (2.10) directly, we can infer that if this vortex lift is coming from the LEV, the contribution will increase with increasing angle of attack up to a saturation limit after which it will remain approximately constant until dropping back to zero as the LEV is shed completely from the leading edge.

2.6. Calculation of the 3D lift curve from first principles

All three models considered in this study are direct functions of the 3D wing lift curve slope at small angles of attack, $C_{L\alpha,3D}$. We evaluate $C_{L\alpha,3D}$ based on the quasi-steady lifting line theory for hovering wings developed by the authors in [37]. The approach provides a good compromise between simplicity and accuracy for lift characterization, and accounts for the necessary physical aspects required to correctly model a steadily revolving wing including: (1) velocity varying as a function of spanwise location, (2) wing planform shape effects including wing chord distribution and aspect ratio, (3) downwash corrections to account for non-uniformity of the developed downwash, and discreteness and periodicity in the wake, and (4) corrections for small aspect ratio relevant to insect-like planforms. For more details of the theory, see [37].

2.7. Comparison of model structures

Before comparing outputs of the three models presented above with experimental data we undertake an objective comparison of the implications of the different model structures. Figure 2 shows a graphical comparison of the models over the whole of the first quadrant of angle of attack ($0–90^{o}$). Also shown here is a nominal experimental representation for a translating wing of the same planform without a LEV. We introduce here a number of transformations (or 'effects') in the $C_L-\alpha$ space associated with well-established classical aerodynamics [47] that helps us relate differences in model behaviour. The first two effects relate to the 2D aerodynamic characteristics of the wing section. These are firstly, the 'flap effect', corresponding to a shift of a lift curve in a direction perpendicular to the lift curve at zero angle of attack, and secondly, the 'slat effect', corresponding to a translation of a lift curve in a direction parallel to the lift curve slope at zero angle of attack. The third effect is related to changes in the overall lift curve slope of the wing, for which planform is normally the driver. We will refer to this as a 'planform effect' as distinct from a 'section effect'. From a modelling point of view, the 'flap effect' is consistent with provision of an increment in circulation at all angles of attack while the 'slat effect' is consistent with an increase in circulation at angles of attack where the maximum lift coefficient, $C_{L,max}$, is limited by stall. Therefore, the 'flap effect' is associated with the 'trapped vortex' model, the 'slat effect' with the 'normal force' model, and the 'planform effect' (between $0 \leq \alpha \leq 45^{\circ}$) with the 'leading edge suction' model.

2.8. Compatibility of models with observed wing pressure distributions

The focus of the present work is on prediction of integrated aerodynamic loads on wings; however, it is also fair to ask to what extent the various models are compatible with the load distributions observed from CFD studies (e.g. [48]). In particular, pressure data show that under some flow conditions there is evidence of a suction foot print consistent

potential flow model	$C_L = C_{L\alpha,3D} \sin\alpha$
normal force model	$C_L = C_{L\alpha,3D} \sin\alpha \cos\alpha$
leading edge suction model	$C_L = C_{L\alpha,3D} \sin\alpha \cos\alpha K_{Pol}(\alpha)$
trapped vortex model	$C_L = C_{L\alpha,3D} \sin\alpha + C_{Lfree,3D}$

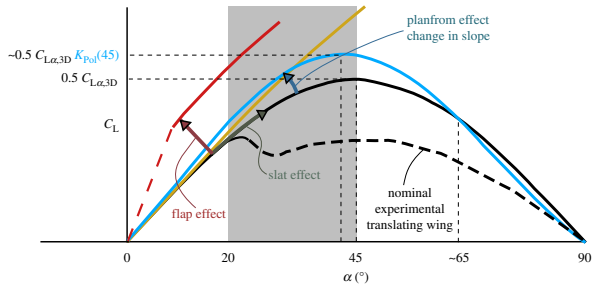

Figure 2. Comparison of the mathematical structure and graphical representation for the models discussed in this study over the first quadrant of angle of attack (potential flow (yellow), normal force (black), leading edge suction (blue) and trapped vortex with $C_{Lfree,3D} > 0$ (red)). All models contain the potential flow model as a component. We choose to show the potential flow model results only up to 45° because this model is known to be non-physical as it approaches 90° angle of attack. Gray band represents typical angle of attack values within the mid-half-strokes of normal hovering insect flight. A nominal experimental representation of a classical stalled translating wing (dashed line) is added for reference.

with that expected from an attached vortex at the leading edge. Given this, we recognize that it is reasonable to expect that the suction from the LEV is directly responsible for at least some of the lift being generated by the wing. However, it seems that the suction footprint is only evident inboard and is relatively small in chordwise extent (see figs 15 and 20 from [48]) and hence in this case the integrated contribution to overall lift is expected to be minor.

3. Comparison of model predictions with experimental and numerical data

3.1. The revolving wing experiment

Before comparing the models to the revolving wing experiment results, we will discuss some essential aspects of the experimental methods used in the literature. Revolving wing experiments are routinely used to simulate flapping wings during the mid-half-stroke wing translational phase. The revolving wing set-up is useful in that it preserves the main steady aerodynamic features of an insect-like flapping wing during mid-half-stroke including the spanwise velocity and pressure gradients as well as the induced effects due to tip vortices. However, it does not capture unsteady aerodynamic effects due to stroke reversals and/or wing–wing interactions that may be important. Nevertheless, the translational aerodynamic mechanism (simulated by the revolving wing set-up) is sufficient to account for weight support production in hovering [15,18,41,49,50]. Eight revolving wing cases from the literature are considered here (table 1). Three different datasets (from three different research groups) are used for the hawkmoth; one dataset is used for each of the bumblebee, the mayfly, the fruitfly, the pigeon and the hummingbird. The wing planforms are defined through the relevant shape parameters: the single-wing aspect ratio, AR,

Table 1. Definition of geometric, experimental and analytical parameters for the datasets used to evaluate LEV models.

	wing description					measurement conditions		analytical values	
species	AR	$\hat{r}_1$[a]	$\hat{r}_2$	$t/\bar{c}$ (%)	material	measurement interval	*Re*	$C_{L\alpha,3D}$	K_{Pol} ($\alpha = 45°$)
hawkmoth HM1 [15]	2.83	0.44	0.511	<1.6	stiffened plastic	$180° - 450°$	8071	2.742	1.15
hawkmoth HM2 [21]	3.09	0.44	0.511[a]	3.7	acrylic	$90° - 270°$	6800	2.863	1.16
hawkmoth HM3 [22]	2.78	0.44	0.511[a]	2	rigid-CFD	$1080° - 1440°$	5400	2.717	1.15
bumblebee BB [16]	3.16	0.477	0.541	—	stiffened plastic[a]	$180° - 450°$	5496	2.813	1.16
mayfly MF [16]	3.21	0.484	0.546	5	stiff card	—	1100	2.816	1.16
fruitfly FF [18,19]	3.3[a]	0.54	0.59[a]	approximately 3[a]	acrylic	arc of 320°	approximately 110	2.677	1.17
pigeon [17]	3.21	0.443	0.512	2.8[a]	card	—	54 000	2.91	1.16
hummingbird HB [20]	4.069	0.43	0.499	—	real wing	—	9800	3.239	1.2

[a]Estimated.

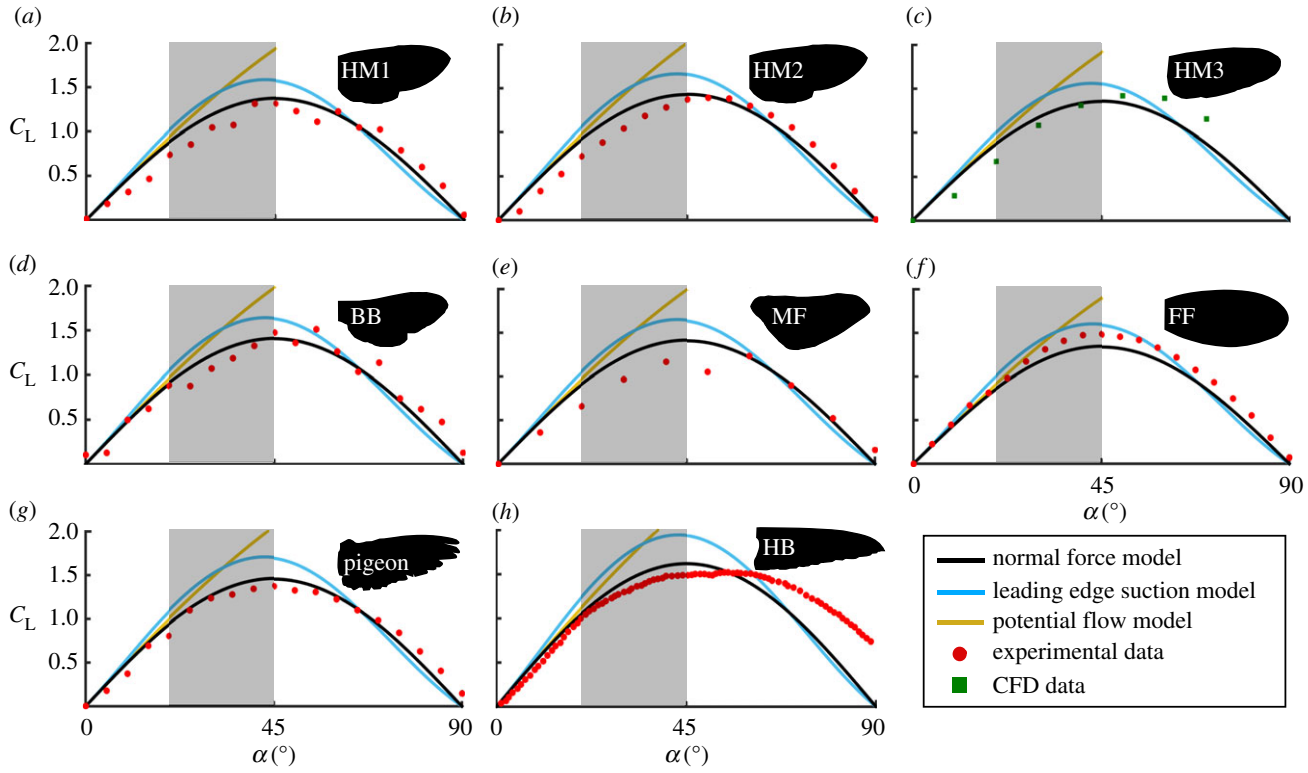

Figure 3. Comparison of aerodynamic model predictions against experimental and CFD data. Lift coefficient data are plotted against geometric angle of attack. Models are compared with available data for (*a*) hawkmoth-1; experimental data digitized from fig. 6 of [15], (*b*) hawkmoth-2; experimental data digitized from fig. 5 of [21], (*c*) hawkmoth-3; CFD data digitized from fig. 5 of [22], (*d*) bumblebee; experimental data digitized from fig. 7 of [16], (*e*) mayfly; experimental data digitized from fig. 8 of [16], (*f*) fruitfly; experimental data digitized from fig. 7 of [19], (*g*) pigeon; experimental data digitized from fig. 3 of [17] and (*h*) hummingbird; experimental data digitized from fig. 6 of [20].

and the non-dimensional radius of the first and second moments of wing area ($\hat{r}_1$ and $\hat{r}_2$, respectively) [51–53,37], which for insect wings are strongly correlated through the relation $\hat{r}_1 = 1.106\hat{r}_2^{1.366}$ [53].

With the exception of the hummingbird wing, the wing section used was an un-cambered flat plate. The thickness to mean chord ratio ($t/\bar{c}$) varies between 1.6% and 5%. While this will have an effect on the zero lift drag coefficient, C_{D0}, the effect on lift coefficient (which is the focus of the present study) is minor. The material used to manufacture each wing is also provided in table 1. This allows qualitative judgement on the degree of rigidity of the used wing models. While all experiments (with the exception of the hummingbird case) assumed rigid wings, this assumption was not perfectly achieved in reality. This can be seen from the non-zero lift values at 90° angle of attack (figure 3). For the hummingbird case, both compliance and camber effects are expected to have affected the measurements; however, these effects are more pronounced at the very high angle of attack range (i.e. $\alpha > 45°$). Thus, we find this a still useful case for comparison particularly for the typical operation angle of attack values up to 45°.

An issue with the available experimental data is the inconsistency of the angular measurement interval provided in table 1. The angular measurement interval corresponds to the wing revolution sector within which the measurement data were collected. Revolving wings may experience a change in the aerodynamic force coefficient values after the first revolution when the wing passes through the disturbed air from the first revolution [22,54]. Additionally, the validity of angular measurement of revolving wing experiments is bounded by the need to allow starting effects to diminish. While absolute values of force coefficients are affected by non-ideal conditions, it is understood that variation of values with angle of attack is relatively unaffected. Hence, with some caution, the lack of consistency in experimental conditions between the validation studies is manageable.

The measurement Reynolds number, *Re*, for each experimental set-up is also provided in table 1. These range from $O(10^2)$ to $O(10^4)$. Experiments [16,19,23] have demonstrated that the dependence of lift coefficient on the Reynolds number in this range is small. A CFD simulation [22] has confirmed this for a higher range of Reynolds number bound up to the $O(10^5)$. On the other hand, Reynolds number does affect the zero lift drag coefficient value, C_{D0} [19,23]. For revolving wings operating at moderate-to-high incidence, the relation $C_D = C_{D0} + C_L\tan(\alpha)$ provides a satisfactory drag coefficient representation. For *Re*, $O(10^3)$ and above, C_{D0} is practically negligible; however, when *Re* is of the $O(10^2)$, C_{D0} seems to have a value around 0.4 [16,18,19,23,38,40].

3.2. Comparison of models with revolving wing data

Figure 3 compares the calculated lift coefficient variation from the modelling approaches presented in §2 within the first quadrant of angle of attack for the eight wing cases. When reviewing the data in figure 3 it should be noted that for normal hovering flight the typical values for the mid-half-stroke angles vary between 20 and 45° [37]. The average errors for the normal force, the leading edge suction, and the potential flow models compared with the experimental

data in this angle of attack range are 11%, 31% and 33%, respectively.

Values of $C_{L\alpha,3D}$ for the eight cases considered in this study are provided in table 1. The leading edge suction model requires further inputs for the values of the *k*-factor contributors k_{ind} and k_{per} within the K_{Pol} term (see equation (2.7)). Values of k_{ind} are based on the approach proposed by the authors in [44]. As for k_{per}, a constant value of 1.1 is assumed for all species considered here. This is based on a previous conclusion that variation of the wake periodicity *k*-factor is minimum and its value is usually clustered around 1.1 [44,51].

4. Discussion

The comparison of models against experimental and numerical data presented in figure 3 shows that the 'normal force' model provides the best fit with respect to both the shape of variation and the amplitude. The 'leading edge suction' model provides a fair fit with respect to the shape of variation of lift against angle of attack; however, it overestimates the lift magnitudes up to an angle of attack value around 65° and then starts to underestimate it. It is noteworthy that the potential lift component of the 'leading edge suction' model, $C_{L,p}$, is a further attenuation of the potential lift, i.e. $C_{L,p}$ = Normal Force Model × cos α. The $\cos^2\alpha$ in the $C_{L,p}$ term was explained by Polhamus to arise from the assumption of a Kutta-type flow condition at the leading edge [55]. However, the application of a Kutta condition at the leading edge was shown to be mathematically invalid by Saffman & Sheffield [46]. This attenuation of the potential lift was compensated for by the addition of vortex lift, $C_{L,v}$; hence allowing recovery of the total lift coefficient value.

The total lift coefficient of the leading edge suction analogy for the angles of attack between 0° and 45° can be regarded as effectively having a higher lift curve slope compared with the 'normal force' model. The difference between the two models is explained with the help of the K_{Pol} term. As shown in table 1, the K_{Pol} term attains values ranging between 1.15 and 1.2 at $\alpha = 45°$ meaning around a 15–20% increase in amplitude compared with the 'normal force' model. It should be noted that the Polhamus model is known to over-predict the wing lift coefficient as the wing aspect ratio increases beyond 1.5. Very good agreement between the Polhamus model and delta wing experimental data of aspect ratios up to 1.5 was shown; however, for an aspect ratio of two, the model over-predicted the experimental lift coefficient values [42]. In addition, the 'leading edge suction' model was only assessed within the typical operation angle of attack range for delta wings ($\alpha \leq 25°$) and its accuracy within the higher angle of attack regime ($25° < \alpha \leq 45°$) was not considered. Therefore, for the wing aspect ratios and angles of attack considered, this difference between the 'leading edge suction' and 'normal force' models is not unexpected.

The potential flow model (i.e. 'trapped vortex' model with zero LEV circulation strength) results in figure 3 become increasingly non-physical at high angles of attack as the model predicts maximum lift at 90° angle of attack whereas the observed lift is zero. However, the model offers good prediction of lift up to around 20° angle of attack, after which it starts to unacceptably over-predict the measurement data. Referring back to equation (2.2), it can be seen that at 45° angle of attack (where the maximum practical lift coefficient is expected to occur) the potential flow model over-predicts the 'normal force' model by a factor of $\sqrt{2}$ (i.e. 41.4% increase in lift coefficient). Despite these concerns, the important result here is that by setting $C_{Lfree,3D}$ to zero in the 'trapped vortex' model, the model still *over-predicts* the lift coefficient. Hence additional circulation from the LEV is not required to predict the observed lift coefficient values.

In conclusion, of the models evaluated, the 'normal force' model provides the best correlation with measured lift values from steadily revolving wings experiencing a LEV, despite the fact that it does not account for additional circulation due to the LEV as in the 'trapped vortex' model, or account for a vortex lift (suction) component as in the Polhamus model. This shows that it is unnecessary to add a specific lift contribution from the LEV to explain the high lift generated in the experimental results. Thus from the two initial hypotheses for the effect of the LEV on lift, we find that improvement in performance via 'absence of stall' is a more satisfying explanation than 'additional lift'.

Data accessibility. This article has no additional data.

Authors' contributions. M.N. conceived the work; M.N. and W.C. developed the models, analysed the results and wrote the paper.

Competing interests. We declare we have no competing interests.

Funding. No funding has been received for this article.

References

1. Sane SP. 2003 The aerodynamics of insect flight. *J. Exp. Biol.* **206**, 4191–4208. (doi:10.1242/jeb.00663)
2. Ellington CP, van den Berg C, Willmott AP, Thomas ALR. 1996 Leading-edge vortices in insect flight. *Nature* **384**, 626–630. (doi:10.1038/384626a0)
3. Shyy W, Liu H. 2007 Flapping wings and aerodynamic lift: the role of leading-edge vortices. *AIAA J.* **45**, 2817–2819. (doi:10.2514/1.33205)
4. Birch JM, Dickinson MH. 2001 Spanwise flow and the attachment of the leading edge vortex on insect wings. *Nature* **412**, 729–733. (doi:10.1038/35089071)
5. Birch JM, Dickson WB, Dickinson MH. 2004 Force production and flow structure of the leading edge vortex on flapping wings at high and low Reynolds numbers. *J. Exp. Biol.* **207**, 1063–1072. (doi:10.1242/jeb.00848)
6. Lentink D, Dickson WB, Van Leeuwen JL, Dickinson MH. 2009 Leading-edge vortices elevate lift of autorotating plant seeds. *Science* **324**, 1438–1440. (doi:10.1126/science.1174196)
7. Bomphrey RJ, Lawson NJ, Harding NJ, Taylor GK, Thomas AL. 2005 The aerodynamics of *Manduca sexta*: digital particle image velocimetry analysis of the leading-edge vortex. *J. Exp. Biol.* **208**, 1079–1094. (doi:10.1242/jeb.01471)
8. Bomphrey RJ, Lawson NJ, Taylor GK, Thomas ALR. 2006 Application of digital particle image velocimetry to insect aerodynamics: measurement of the leading-edge vortex and near wake of a Hawkmoth. *Exp. Fluids* **40**, 546–554. (doi:10.1007/s00348-005-0094-5)
9. Bomphery RJ, Taylor GK, Thomas ALR. 2009 Smoke visualization of free-flying bumblebees indicates independent leading edge vortices on each wing pair. *Exp. Fluids* **46**, 811–821. (doi:10.1007/s00348-009-0631-8)
10. Warrick DR, Tobalske BW, Powers DR. 2005 Aerodynamics of the hovering hummingbird. *Nature* **435**, 1094–1097. (doi:10.1038/nature03647)
11. Warrick DR, Tobalske BW, Powers DR. 2009 Lift production in the hovering hummingbird.

Proc. R. Soc. Lond. B **276**, 3747–3752. (doi:10.1098/rspb.2009.1003)

12. Muijres FT, Johansson LC, Barfield R, Wolf M, Spedding GR, Hedenström A. 2008 Leading-edge vortex improves lift in slow-flying bats. *Science* **319**, 1250–1253. (doi:10.1126/science.1153019)
13. Muijres FT, Johansson LC, Hedenström A. 2012 Leading edge vortex in a slow-flying passerine. *Biol. Lett.* **8**, 554–557. (doi:10.1098/rsbl.2012.0130)
14. Videler JJ, Stamhuis EJ, Povel GDE. 2004 Leading-edge vortex lifts swifts. *Science* **306**, 1960–1962. (doi:10.1126/science.1104682)
15. Usherwood JR, Ellington CP. 2002 The aerodynamics of revolving wings: I. Model hawkmoth wings. *J. Exp. Biol.* **205**, 1547–1564.
16. Usherwood JR, Ellington CP. 2002 The aerodynamics of revolving wings: II. Propeller force coefficients from mayfly to quail. *J. Exp. Biol.* **205**, 1565–1576.
17. Usherwood JR. 2009 The aerodynamic forces and pressure distribution of a revolving pigeon wing. *Exp. Fluids* **46**, 991–1003. (doi:10.1007/s00348-008-0596-z)
18. Dickson WB, Dickinson MH. 2004 The effect of advance ratio on the aerodynamics of revolving wings. *J. Exp. Biol.* **207**, 4269–4281. (doi:10.1242/jeb.01266)
19. Lentink D, Dickinson MH. 2009 Rotational accelerations stabilizes leading edge vortices on revolving fly wings. *J. Exp. Biol.* **212**, 2705–2719. (doi:10.1242/jeb.022269)
20. Kruyt JW, Quicazán-Rubio EM, van Heijst GF, Altshuler DL, Lentink D. 2014 Hummingbird wing efficacy depends on aspect ratio and compares with helicopter rotors. *J. R. Soc. Interface* **11**, 20140585. (doi:10.1098/rsif.2014.0585)
21. Han JS, Kim JK, Chang JW, Han JH. 2015 An improved quasi-steady aerodynamic model for insect wings that considers movement of the center of pressure. *Bioinspir. Biomim.* **10**, 046014. (doi:10.1088/1748-3190/10/4/046014)
22. Guo X, Chen D, Liu H. 2015 Does a revolving wing stall at low Reynolds numbers? *J. Biomech. Sci. Eng.* **10**, 15–00588. (doi:10.1299/jbse.15-00588)
23. Ellington CP. 2006 Insects versus birds: the great divide. In *44th AIAA Aerospace Sciences Meeting and Exhibit*, AIAA-2006-35, pp. 450–455. (doi:10.2514/6.2006-35)
24. Pitt Ford CW, Babinsky H. 2013 Lift and the leading-edge vortex. *J. Fluid Mech.* **720**, 280–313. (doi:10.1017/jfm.2013.28)
25. Stevens RJ *et al.* 2016 Low Reynolds number acceleration of flat plate wings at high incidence. In *54th AIAA Aerospace Sciences Meeting*, AIAA 2016-0286. (doi:10.2514/6.2016-0286)
26. Jones AR, Manar F, Phillips N, Nakata T, Bomphrey R, Ringuette MJ, Percin M, van Oudheusden B, Palmer J. 2016 Leading edge vortex evolution and lift production on rotating wings. In *54th AIAA Aerospace Sciences Meeting*, AIAA 2016-0288. (doi:10.2514/6.2016-0288)
27. Babinsky H, Stevens RJ, Jones AR, Bernal LP, Ol MV. 2016 Low order modelling of lift forces for unsteady pitching and surging wings. In *54th AIAA Aerospace Sciences Meeting*, AIAA 2016–0290. (doi:10.2514/6.2016-0290)
28. Phillips N, Knowles K, Bomphrey RJ. 2017 Petiolate wings: effects on the leading-edge vortex in flapping flight. *Interface Focus* **7**, 20160084. (doi:10.1098/rsfs.2016.0084)
29. Lee YJ, Lua KB, Lim TT. 2016 Aspect ratio effects on revolving wings with Rossby number consideration. *Bioinspir. Biomim.* **11**, 056013. (doi:10.1088/1748-3190/11/5/056013)
30. Maxworthy T. 1979 Experiments on the Weis-Fogh mechanism of lift generation by insects in hovering flight. Part 1. Dynamics of the 'fling'. *J. Fluid Mech.* **93**, 47–63. (doi:10.1017/S0022112079001774)
31. McCroskey WJ. 1981 *The phenomenon of dynamic stall*. NASA Technical Memorandum TM-81264.
32. Ansari SA, Żbikowski R, Knowles K. 2006 Aerodynamic modelling of insect-like flapping flight for micro air vehicles. *Prog. Aerosp. Sci.* **42**, 129–172. (doi:10.1016/j.paerosci.2006.07.001)
33. Kruyt JW, van Heijst GF, Altshuler DL, Lentink D. 2015 Power reduction and the radial limit of stall delay in revolving wings of different aspect ratio. *J. R. Soc. Interface* **12**, 20150051. (doi:10.1098/rsif.2015.0051)
34. Ormiston RA. 2004 Induced power of the helicopter rotor. In *American Helicopter Society 60th Annual Forum and Technology Display, Baltimore, MD, USA, 8–10 June 2004*, pp. 33–53.
35. Chattot JJ. 2004 Analysis and design of wings and wing/winglet combinations at low speeds. In *42nd AIAA Aerospace Sciences Meeting and Exhibit*, AIAA 2004-220. (doi:10.2514/6.2004-220)
36. Nabawy MRA, Crowther WJ. 2014 On the quasi-steady aerodynamics of normal hovering flight part II: model implementation and evaluation. *J. R. Soc. Interface* **11**, 20131197. (doi:10.1098/rsif.2013.1197)
37. Nabawy MRA, Crowther WJ. 2015 A quasi-steady lifting line theory for insect-like hovering flight. *PLoS ONE* **10**, e0134972. (doi:10.1371/journal.pone.0134972)
38. Nabawy MRA, Crowther WJ. 2015 Aero-optimum hovering kinematics. *Bioinspir. Biomim.* **10**, 044002. (doi:10.1088/1748-3190/10/4/044002)
39. Deng X, Schenato L, Wu, WC, Sastry SS. 2006 Flapping flight for biomimetic robotic insects: Part I-system modeling. *IEEE Trans. Robot.* **22**, 776–788. (doi:10.1109/TRO.2006.875480)
40. Berman GJ, Wang ZJ. 2007 Energy-minimizing kinematics in hovering insect flight. *J. Fluid Mech.* **582**, 153–168. (doi:10.1017/S0022112007006209)
41. Taha HE, Hajj MR, Beran PS. 2014 State-space representation of the unsteady aerodynamics of flapping flight. *Aerosp. Sci. Technol.* **34**, 1–11. (doi:10.1016/j.ast.2014.01.011)
42. Polhamus EC. 1966 A concept of the vortex lift of sharp-edge delta wings based on a leading-edge-suction analogy. NASA Technical Note D-3767.
43. Traub LW. 2004 Analysis and estimation of the lift components of hovering insects. *J. Aircraft* **41**, 284–289. (doi:10.2514/1.9323)
44. Nabawy MRA, Crowther WJ. 2014 On the quasi-steady aerodynamics of normal hovering flight part I: the induced power factor. *J. R. Soc. Interface* **11**, 20131196. (doi:10.1098/rsif.2013.1196)
45. Ahmed MR, Abdelrahman MM, ElBayoumi GM, ElNomrossy MM. 2011 Optimal wing twist distribution for roll control of MAVs. *Aeronaut. J.* **115**, 641–649. (doi:10.1017/S0001924000006333)
46. Saffman PG, Sheffield JS. 1977 Flow over a wing with an attached free vortex. *Stud. Appl. Math.* **57**, 107–117. (doi:10.1002/sapm1977572107)
47. O. Smith AM. 1975 High-lift aerodynamics. *J. Aircraft.* **12**, 501–530. (doi:10.2514/3.59830)
48. Harbig RR, Sheridan J, Thompson MC. 2013 Relationship between aerodynamic forces, flow structures and wing camber for rotating insect wing planforms. *J. Fluid Mech.* **730**, 52–75. (doi:10.1017/jfm.2013.335)
49. Sane SP, Dickinson MH. 2002 The aerodynamic effects of wing rotation and a revised quasi-steady model of flapping flight. *J. Exp. Biol.* **205**, 1087–1096.
50. Wang ZJ. 2005 Dissecting insect flight. *Annu. Rev. Fluid Mech.* **37**, 183–210. (doi:10.1146/annurev.fluid.36.050802.121940)
51. Nabawy MRA, Crowther WJ. 2014 Is flapping flight aerodynamically efficient? In *32nd AIAA Applied Aerodynamics Conf., AIAA Aviation and Aeronautics Forum and Exposition, Atlanta, GA, USA, 16–20 June 2014*. (doi:10.2514/6.2014-2277)
52. Nabawy MRA, Crowther WJ. 2016 Optimum hovering wing planform. *J. Theor. Biol.* **406**, 187–191. (doi:10.1016/j.jtbi.2016.06.024)
53. Ellington CP. 1984 The aerodynamics of hovering insect flight. II. Morphological parameters. *Phil. Trans. R. Soc. Lond. B* **305**, 17–40. (doi:10.1098/rstb.1984.0050)
54. Venkata SK, Jones AR. 2013 Leading-edge vortex structure over multiple revolutions of a rotating wing. *J. Aircraft* **50**, 1312–1316. (doi:10.2514/1.C032128)
55. Polhamus EC. 1968 Application of the leading-edge-suction analogy of vortex lift to the drag due to lift of sharp-edge delta wings. NASA Technical Note D-4739.